https://doi.org/10.1016/j.cemconres.2021.106582

Understanding geopolymer binder-aggregate interfacial characteristics at molecular level

Ming-Feng Kai and Jian-Guo Dai*

1. Post-doctoral Fellow, Department of Civil and Environmental Engineering, The Hong Kong Polytechnic University, Hong Kong, Email: mingfeng.kai@polyu.edu.hk, ORCID: 0000-0002-7626-2328
2. Professor (Corresponding author), Department of Civil and Environmental Engineering, The Hong Kong Polytechnic University, Hong Kong, Email: cejgdai@polyu.edu.hk, ORCID: 0000-0001-9904-7914

Abstract

The interfacial characteristics of geopolymer binder to aggregate composites are poorly understood, especially at molecular level. Herein, molecular models are developed to study, for the first time, the geopolymer-aggregate interface. Chemically, various forms of interfacial bonding are characterized, including Al-O-Si bonding through condensation reactions, Na-O and H-bonding. An atomic-level interfacial transition zone (ITZ) is identified, attributed to the concentration of –OH groups. Increasing the Si/Al ratio of geopolymer is found to decrease the ITZ density, but have limited effect on the ITZ width. A heterogeneous diffusion characteristic occurs in geopolymer, due to the weak interfacial interaction. Mechanically, lowering the Si/Al ratio promotes the interfacial strength due to the stronger interfacial interaction and higher cross-linking degree in geopolymer. Under loading the interfacial fracture undergoes three stages: crack propagation, chain bridging (including aluminosilicate and ionic bridging) and breakage. The above atomic-level findings may facilitate a better design of geopolymer concrete in engineering.

Keywords: Chemical bonding; Interfacial transition zone; Heterogeneous diffusion characteristic; Interfacial strength; Interfacial fracture

1. Introduction[U1]

Cement industry is facing a huge challenge to meet the requirements of sustainable development, as it contributes about 6−8% emissions of human-made CO_2 all over the world [1-3]. Therefore, there is an urgent need to look for more environmentally friendly cement binding materials for sustainable construction. As a kind of alkali-activated binder, geopolymer has drawn considerable attention from both academia and industry as a promising sustainable alternative to ordinary Portland cement (OPC). A wide variety of source materials can be used for the geopolymer synthesis, including metakaolin, fly ash, calcined clay, furnace slag, mine tailings [4-7]. Besides, biomass wastes such as rice husk ash and wood ash have been recycled as the precursor materials [8-10]. The geopolymer synthesis generally involves two processes: (1) the dissolution of source materials composed of aluminosilicate minerals under the alkali environment (e.g. NaOH and KOH solutions) to release small molecules known as oligomers; and (2) the condensation of these aluminosilicate oligomers into a covalently bonded network [11-13]. According to the Si/Al atomic ratio, geopolymer comprises different chemical units: -Si-O-Si-O- (siloxo), -Si-O-Al-O- (sialate), -Si-O-Al-O-Si-O- (sialate-siloxo) and -Si-O-Al-O-Si-O-Si-O- (sialate-disiloxo). Besides environmental advantages (e.g. over 80% reduction in CO_2 emission and reuse of industrial waste [8, 14]), geopolymer poses tunable strength at both early and later ages, better durability, improved acid resistance, and higher temperature/fire resistance [15]. Because of these advantageous properties, geopolymer concrete has a good potential to become an alternative to conventional OPC concrete in many applications and is especially attractive to some special fields that demand extreme properties, such as toxic/radioactive waste encapsulation, fire resistant coatings and sewage pipes [16-18].

An important issue for geopolymer concrete is to understand the interfacial behavior (both chemically and physically) between the geopolymer binder and the aggregates. In recent years, a few experimental studies have been carried out to characterize the interfacial microstructure and the binding behaviors in geopolymer concrete. Sarker et al. [19] and Peng et al. [20] reported that geopolymer concrete shows a higher tensile strength than OPC concrete given the same compressive strength, originating from the stronger bond strength at the interface between

the geopolymer binder and aggregates. Khan et al. [21] proposed that the incorporation of CaO and MgO into the geopolymer results in a stronger bond between the geopolymer matrix and the aggregates. Pacheco-Torgal et al. [12] employed schist sand, granite and limestone as the aggregates and detected the interfacial microstructures in geopolymer concrete. In contrast with the typical porous interfacial transition zone (ITZ) of cement mixtures, a very dense and uniform ITZ was observed independent of the aggregate type, which is likely due to the better chemical interaction between the paste and aggregates. Also, the existence of ITZ in geopolymer concrete was confirmed by Khan et al. [21], Demie et al. [22], Sarker et al. [19], and Embong et al. [23]. However, some researchers claimed that no obvious ITZ was identified in geopolymer concrete, as there is no apparent difference between the bulk geopolymer matrix and microstructures of the ITZ [24-27]. Despite all of these existing efforts, the interfacial chemical structure of geopolymer concrete remains elusive because current experimental techniques (e.g. scanning electron microscopy, X-ray diffraction, energy-dispersive X-ray spectroscopy, Fourier transform infrared spectroscopy, nuclear magnetic resonance) can neither provide insights into the geopolymerization process at molecular level nor qualitatively identify the chemical composition of the geopolymer binder at the interface [28-30].

Molecular dynamics (MD), bypassing the experimental difficulties, could contribute a deep insight into the chemical and physical basis of materials at molecular level [31-33]. Previously, Lolli et al. [34] developed geopolymer atomic models based on a defective crystal structure to describe the geopolymerization product of sodium silicate-activated metakaolin. Zhang et al. [28] carried out, perhaps for the first time, a reactive MD simulation of the polymerization process of aluminosilicates for geopolymer synthesis, which produced realistic geopolymer models comparable to experimentally synthesized geopolymer. Following this method, Zhang et al. [35, 36] developed geopolymer models to study the chemical interactions between active geopolymer and nano-materials. Up to now, the MD tool has been widely applied to study the interfacial properties in various composite systems. For example, MD simulation reveals that the interfacial bonding between asphalt and aggregate is strongly dependent on the types of chemical compounds and functional groups (e.g. saturates, aromatics,

resins, and asphaltenes) in the asphalt binder [37-41], and the interfacial failure is affected by many factors, such as moisture content [39, 40, 42, 43], air void [44, 45], loading rate [44, 45], aging [40, 41] and temperature [38, 44-46]. Besides, the MD tool has been used to study the interfacial properties of many other composites, such as water-silica [47], water-metal [48], polymer-silica [49], polymer-metal [50], coating-metal [51] and solution-mineral [52].[U2] These studies facilitated a better understanding of the physics and chemistry at the interfaces, which are usually not accessible experimentally. To the best of the authors' knowledge, however, there is still no atomic-level study on the interfacial characteristics of geopolymer concrete system, especially considering the formation of the interfacial chemical structure and the effect of the Si/Al ratios of geopolymer binder.

In this study, a reactive MD simulation is carried out, for the first time, to provide atomic-level insights into the interfacial characteristics between geopolymer binder and silica aggregates, considering three typical Si/Al ratios of geopolymer. First, the potential chemical reactions between geopolymer and aggregate are explored and the effect of Si/Al ratios is discussed, following which the interfacial structure is characterized to find how the ITZ exists and the corresponding features. Then, atom trajectories are recorded to analyze the diffusion behavior of geopolymer onto the aggregate surface. Mechanically, the interfacial strength is tested using a strain constant method and the full-range fracture process is captured.

2. Simulation Method

2.1 Model establishment

Considering the main chemical components in aggregates are sand, granite, quartz, and basalt, a silica (SiO_2-alpha) unit is often selected to build a representative aggregate model [43, 44, 53]. The initial silica model is a monoclinic cell with a size of a = 4.91 Å, b = 4.91 Å, c = 5.41 Å ($\alpha = 90^o$, $\beta = 90^o$, $\gamma = 120^o$), as shown in Fig. 1(a). To begin with, a (8 × 10 × 8) supercell of silica is transformed into an orthorhombic configuration with a size of 39.30 Å × 42.55 Å × 43.24 Å [37]. To construct the geopolymer binder-aggregate interface, an exposed silica surface is created by introducing a 40 Å vacuum gap perpendicular to the (010) direction. Hydroxyl groups are assigned on the surface to represent its hydrated form (≡Si-OH), which is

in line with the experimental finding that one hydroxyl group per one surface Si is the most probable form on the fully hydroxylated silica surface [54, 55]. As the polymerization of geopolymer starts with oligomers, 440 sialate oligomers (Fig.1 a) together with the same number of Na atoms (for charge balance) are packed into the vacuum region as the initial geopolymer model with a Si/Al = 1, as shown in Fig. 1(b). To design the geopolymer models with different Si/Al ratios, partial sialate units in geopolymer are replaced by siloxo units (Fig. 1a) to achieve Si/Al ratios of 2 and 3 [36, 56], as shown in Fig. 1(c) and (d). The number of Na atoms in the geopolymer system is consistent with that of Al atoms. As a result, three geopolymer-aggregate composite models are prepared with three typical Si/Al ratios.

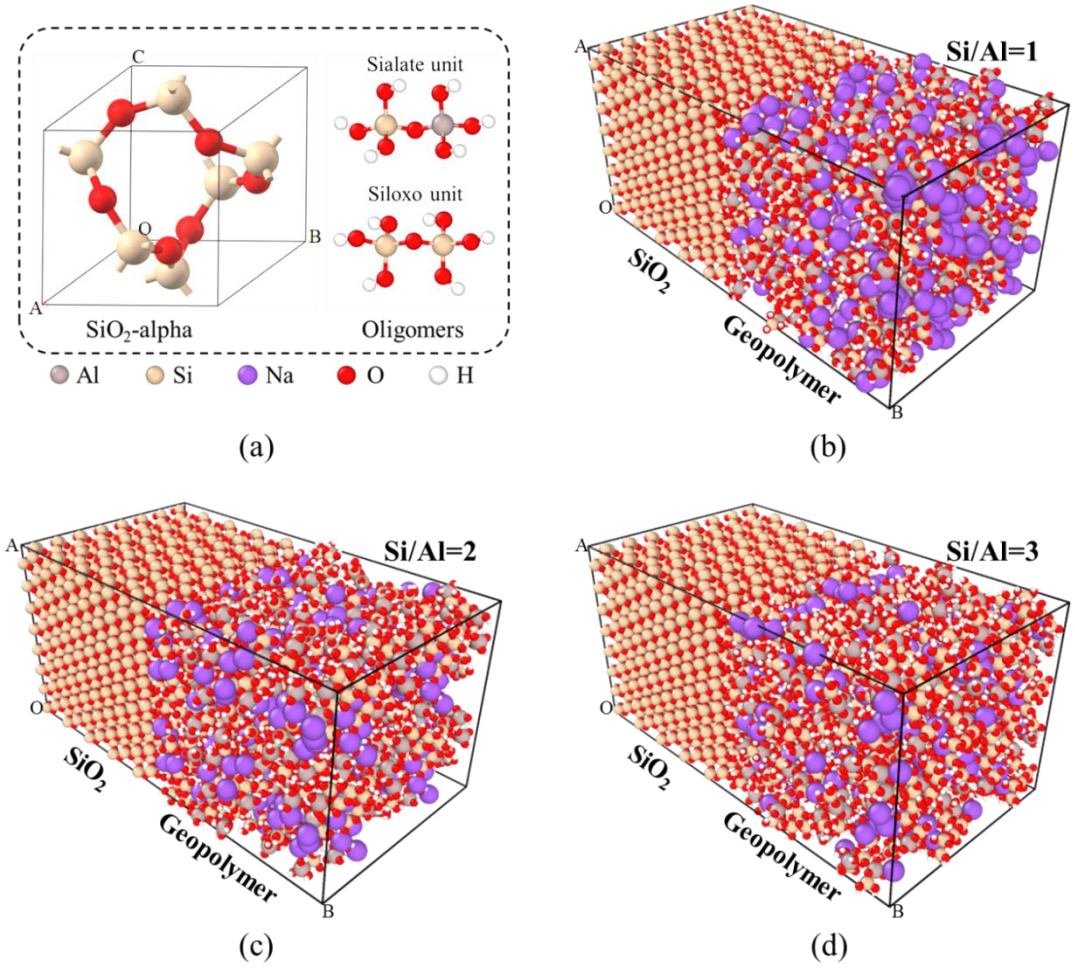

Fig. 1 (a) Initial atomic models for fabricating silica aggregate and geopolymer: SiO_2-alpha unit cell, sialate and siloxo oligomers (Here we use ball-and-stick models to show the connection between atoms); (b-d) a perspective view of geopolymer-aggregate composite models with typical Si/Al ratios of 1, 2 and 3 (Here

we use CPK models, also known as “space-filling model”, to show the atoms whose radii are proportional to the radii of the atoms).

2.2 Simulation procedure

First, the initial composite models are geometry-optimized based on the conjugate gradient (CG) algorithm with a convergence criterion of 10^{-6} kcal/mol, followed by a dynamic equilibration for 300 ps under the isothermal-isobaric (NPT) ensemble with a temperature of 300 K (room temperature) and a pressure of 101 kPa (atmospheric pressure). The Nose-Hoover thermostat and barostat algorithms are applied for the temperature and pressure control [57, 58]. Then, these composite systems are thermally treated at 1500 K for 300 ps under the canonical (NVT) ensemble to accelerate the polymerization of the oligomers, which is a common method to produce a realistic cross-linked geopolymer model [28, 35, 36, 56]. During the thermal treatment, water molecules produced by the polymerization are removed in case of the formation of voids in geopolymer caused by the agglomeration of too many water molecules as the capillary water [28, 35, 56, 59]. These models are gradually cooled down to 300 K with a cooling rate of 5 K/ps. Subsequently, the Grand Canonical Monte Carlo (GCMC) method is performed to absorb water molecules into the dry cross-linked geopolymer models as the physically absorbed water. The final water contents are 7.9 %, 8.0 % and 8.1 % by weight of geopolymer with Si/Al ratios of 1, 2 and 3 respectively, which are close to the reported values (7.9 % in Ref. [36] and 7.64 % in Ref. [60]). After the GCMC process, a further dynamic equilibrium is carried out for another 300 ps under the NPT ensemble with a temperature of 300 K and pressure of 101 kPa.

A structural analysis of these final geopolymer-aggregate composite models is carried out to explore the interfacial molecular structures and the effect of Si/Al ratio. In order to study the atom dynamics of different components, including aluminosilicates, Na^+ ions and water molecules, in geopolymer matrices, the trajectory information of atoms is recorded by further equilibrating these systems for 500 ps under the NVT ensemble at 300 K. To investigate the interfacial mechanical properties and fracture process of these composites, a uniaxial tensile loading is applied on the composite models along the y-direction (perpendicular to the

interfaces), before which a small defect with a size of 9 Å width and 5 Å thickness is introduced on the silica surface to induce the interfacial defect propagation, as shown in Fig. 2(a). Fig. 2(b) shows a schematic view of the defect design by deleting some atoms on the surface of silica aggregate and assigning hydroxyl groups on the newly exposed surface. The uniaxial tensile loading is applied using a constant-strain method with a strain rate of 0.01%/ps, indicating that the model dimension along the y-direction changes linearly with time. The strain rate employed in this study has been widely suggested to measure the stress-strain curves of various inorganic systems in MD simulation. During the tensile loading, the NPT ensemble with a temperature of 300 K is implemented and the pressure is controlled at 101 kPa in x and z directions to take account of the Poisson effect.

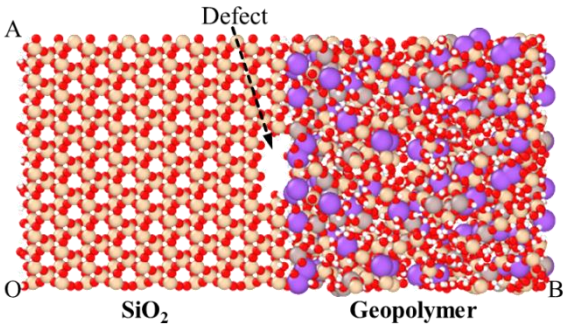

(a) Side view of a composite model for tension

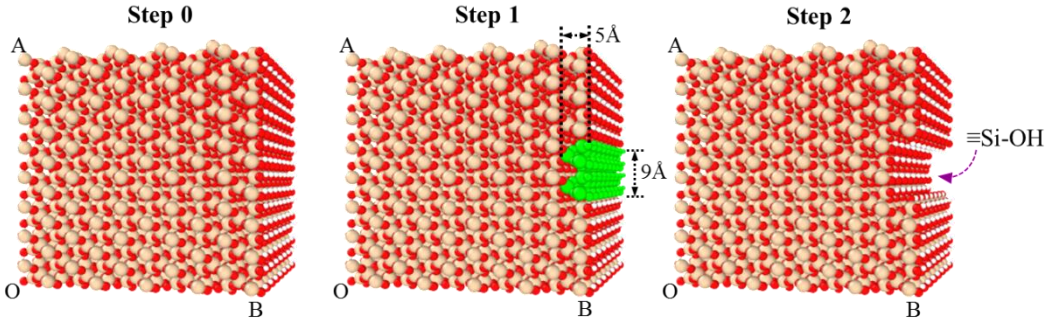

(b) A schematic view of the defect design on SiO_2 surface

Fig. 2 (a) A side view of a composite model with a small defect designed for the tensile test along y direction; (b) A schematic view of the defect design on SiO_2 aggregate surface (Step 0: a defect-free SiO_2 surface; Step 1: selection of the atoms within the middle region (9 Å × 5 Å) in the xy plane, which are labeled with green color; Step 2: removal of green atoms and hydrogenation of new exposed O atoms for charge balance.

All the simulations are carried out using the Large-scale Atomic/Molecular Massively

Parallel Simulator (LAMMPS) software with a time step of 0.25 fs. Periodic boundary conditions are applied to all directions of the composite systems during all the simulation processes mentioned above. Therefore, both sides (perpendicular to the y-direction) of silica aggregate can interact with geopolymer: one is in the middle, and the other is at the boundary.

2.3 Reactive force field

In this study, the reactive force field (ReaxFF), developed by van Duin et al. [61] for use in MD simulations, is employed to express both inter- and intra-molecular interactions. This force field uses the distance-dependent bond order concept to describe the instantaneous interactions between atoms, which allows for a smooth transition between the bonded states (including single, double, or triple bonds) and un-bonded states. This strategy allows one to simulate the chemical processes where the bond formation and dissociation are involved during the dynamic evolution of a system. In general, the ReaxFF divides the system total energy (E_{system}) into several partial contributions, as given below [62],

$$E_{Total} = E_{bond} + E_{over} + E_{under} + E_{val} + E_{tor} + E_{lp} + E_{H\text{-}bond} + E_{vdW} + E_{coul} \quad (1)$$

where E_{bond} is the two-body energies associated with bonded atoms; E_{over} and E_{under} are the penalty energies preventing the atom over/under-coordination; E_{val} and E_{tor} are the energies correlated with three-body valence angle strain and four-body torsional angle strain, respectively; E_{lp} is the lone-pair energies based on the number of lone pairs around an atom; $E_{H\text{-}bond}$ is the hydrogen-bond (H-bond) energies; E_{vdW} and E_{coul}, are van der Waals and Coulomb contributions calculated between all the atom pairs regardless of connectivity, and includes a shielding parameter to avoid excessive repulsion at short distances. The atomic charges are adjusted at each MD time step using the Charge equilibration (QEq) scheme. More details about these partial energy terms in ReaxFF can be found elsewhere [63].

The ReaxFF parameters employed in this work were developed by the group of van Duin [64]. These parameters have been fit to a large quantum mechanics (QM) training set containing data of Na/Si/Al/O/H systems, via a single-parameter search optimization to minimize the error,

so that the ReaxFF MD simulation can retain accuracy nearly as great as that of QM calculations [63]. Previously, these parameters have already been successfully applied to study a variety of materials, such as silica [65, 66], geopolymer [35, 59], zeolite [64, 67], clay minerals [68, 69], calcium silicate hydrates [70, 71], sodium aluminosilicate glass [72, 73].

3. Results and Discussion

3.1 Interfacial bonding and structure

To understand the interfacial chemical structures, it is necessary to figure out the chemical interaction between the geopolymer and the silica aggregate firstly. By observing the formation process of the interfacial chemical structure, it is found that active aluminosilicate oligomers can react with silica aggregate by typical condensation reactions, as illustrated in Fig. 3(a). Initially, four-coordinated Al (Al[4]) in oligomers is coordinated with an oxygen atom in the hydroxyl group exposed on the surface of the aggregate. At this intermediate state, Al[4] is transformed into five-coordinated Al (Al[5]) and a Brønsted acid site (proton donor) is formed [74]. Next, the Brønsted acid site donates the H^+, which further binds with one adjacent OH^- ion to produce a H_2O molecule coordinated with Al[5]. Finally, the H_2O molecule can escape from Al[5] coordination and diffuse in geopolymer. At this state, Al[5] is transformed back into Al[4]. As a result, an interfacial Al-O-Si bonding (type 1) is formed. It is also found that ≡Al-OH groups in the oligomers chemically bonded with aggregate can further polymerize with adjacent ≡Si-OH groups from the aggregate by the same condensation reaction mechanism, resulting in a new type Al-O-Si bonding (type 2) between the geopolymer and the aggregate, as illustrated in Fig. 3(b). Similarly, it is found that geopolymer can chemically bond with various materials due to its activity, such as Al-O-Fe bonding with steel [75], Al-O-C bonding with catechol in humic substances [76], and Al-O-Si bonding with Si-doped graphene [62]. In addition, there exists ionic (Na-O) bonding and H-bonding that bridge the geopolymer and the silica aggregate, as illustrated in Fig. 3(c). For the H-bonding, it can be formed between –OH groups in aluminosilicates and aggregate or formed by H_2O. In conclusion, there are various forms of interfacial chemical bonding between geopolymer and silica aggregate, including two types of Al-O-Si bonding through condensation reactions, Na-O ionic bonding

and H-bonding.

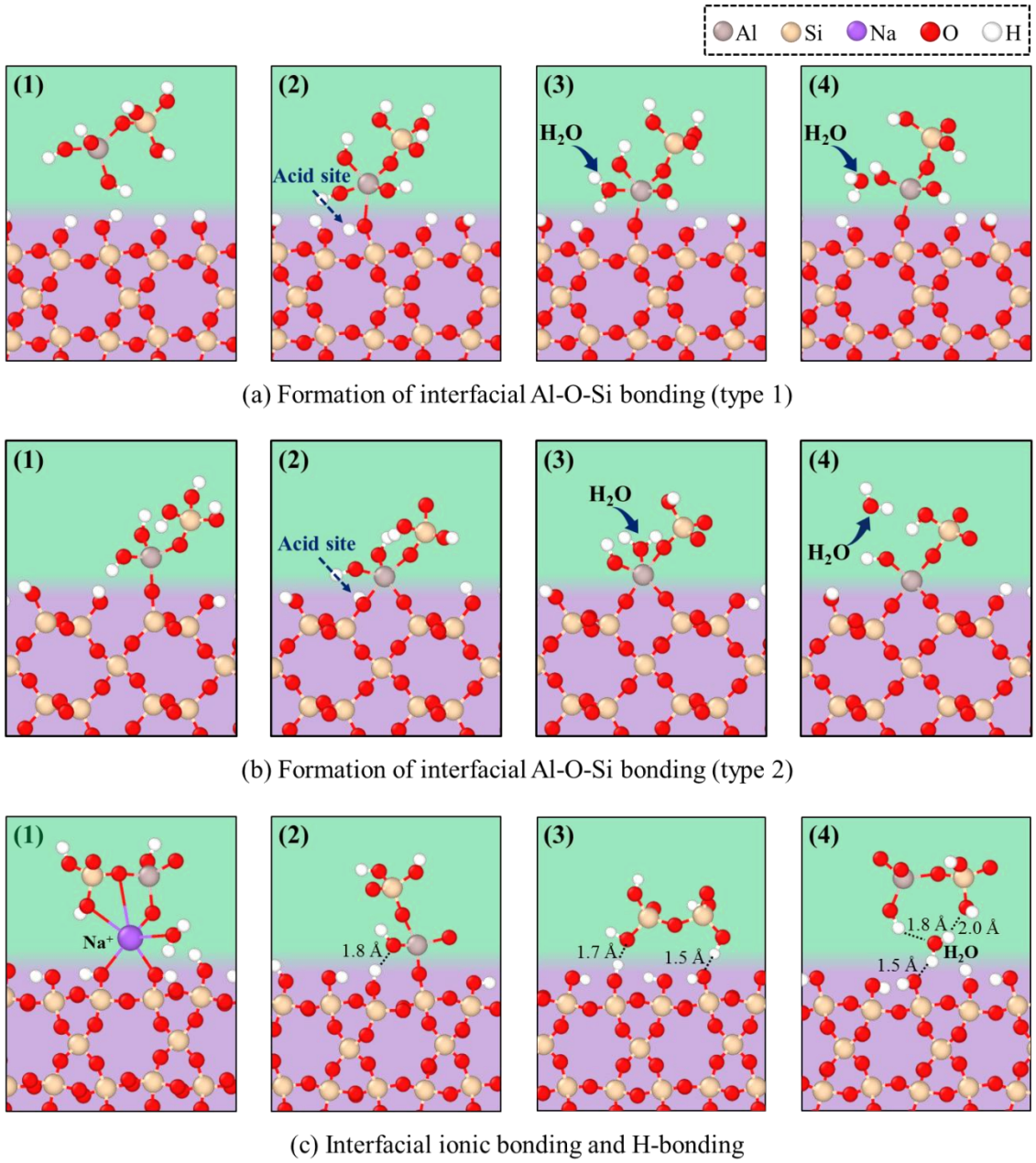

Fig. 3 Snapshots of the interfacial chemical bonding between geopolymer and silica aggregate: (a) formation of type 1 Al-O-Si bonding; (b) formation of type 2 Al-O-Si bonding; (c.1) Na-O ionic bonding and (c.2-4) Multiform H-bonding.

To further understand the interfacial chemical structures, the concentrations of different interfacial chemical bonds are calculated, which are defined as the number of chemical bonds divided by the surface area of the aggregate, as shown in Fig. 4 (a). At the interfaces, the bond

concentration follows an order of Al-O-Si < Na-O < H-bond. The concentrations of interfacial Al-O-Si and Na-O bonds are 1.14 nm^{-2} and 2.74 nm^{-2} respectively for geopolymer (Si/Al =1). With Si/Al ratio rising to 3, the interfacial bond concentrations for these two types of bonds decrease by nearly a half. However, the interfacial H-bond concentration is hardly affected by Si/Al ratio. As depicted in Fig. 3(c), the interfacial H-bonding can be formed by aluminosilicates and water with silica aggregate. To distinguish these two different H-bonding at the interface, the contributions to the H-bond from aluminosilicates and water with the silica aggregate is calculated, as shown in Fig. 4(b). The H-bond between aluminosilicates and aggregate contributes to 61%~66% of the total interfacial H-bonds while that between water and aggregate contributes to the remaining 34%~39% in various geopolymer-aggregate composites, indicating that the interfacial H-bonds mainly originate from the aluminosilicates on the aggregate surface.

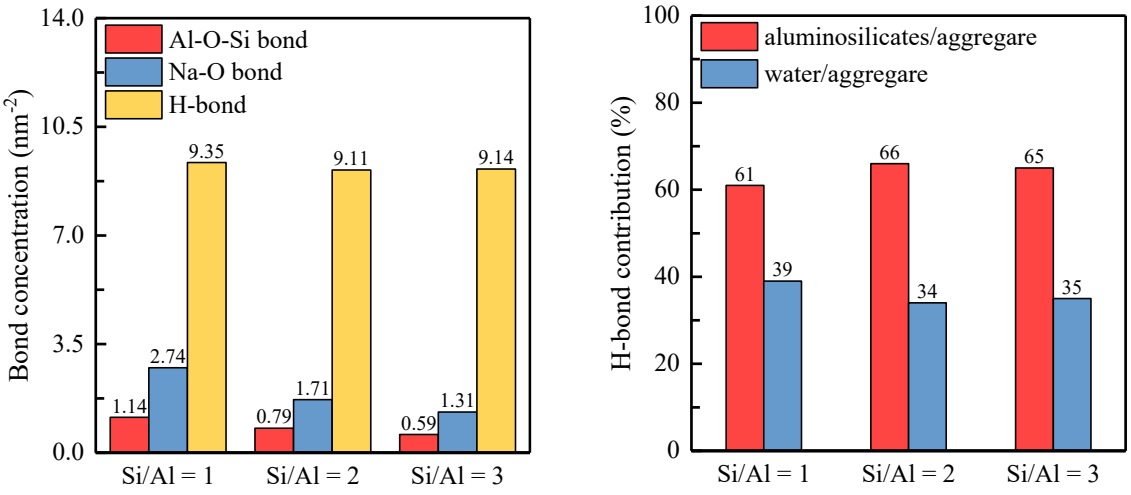

Fig. 4 (a) The concentration of various interfacial chemical bonds (Al-O-Si, Na-O and H-bond) between geopolymer and silica aggregate; (b) the interfacial H-bond contribution (%) from aluminosilicates and water in geopolymer with silica aggregate.

It is well-known that geopolymer has a cross-linked aluminosilicate structure; as a result, the polymerization of the aluminosilicate oligomers is realized through a typical condensation reaction [28]. Fig. 5(a) shows a snapshot of the cross-linked geopolymer model built in this

study and its internal cross-linking between oligomers. The condensation reaction between ≡Al-OH and ≡Si-OH groups from oligomers results in the formation of Si-O-Al link between oligomers while the formation of Al-O-Al link is attributed to the condensation reaction between two ≡Al-OH groups. The bridging oxygen is usually called cross-linking sites [77, 78], which is marked with green in Fig. 5. It is also observed that partial Al[4] in geopolymer is transformed into Al[5], which is in line with the experimental analysis of geopolymer materials from ^{27}Al magic angle spinning nuclear magnetic resonance (MAS NMR) [79]. Fig. 5(b) depicts the cross-linking sites in geopolymer with various Si/Al ratios. Obviously, the increase in Si/Al ratios reduces the number of cross-linking sites from 659 to 375, indicating that the aluminosilicates in geopolymer are more highly cross-linked at lower Si/Al ratios, attributed to more active ≡Al-OH groups participating in the condensation reaction. Similarly, it was found that higher Al content in geopolymer can promote the polymerization process [28], in consistent with the present findings.

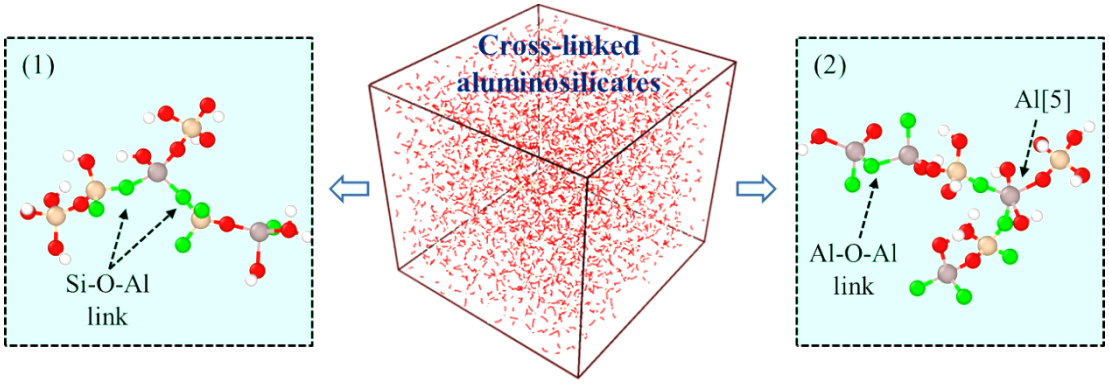

(a) Cross-linked aluminosilicates

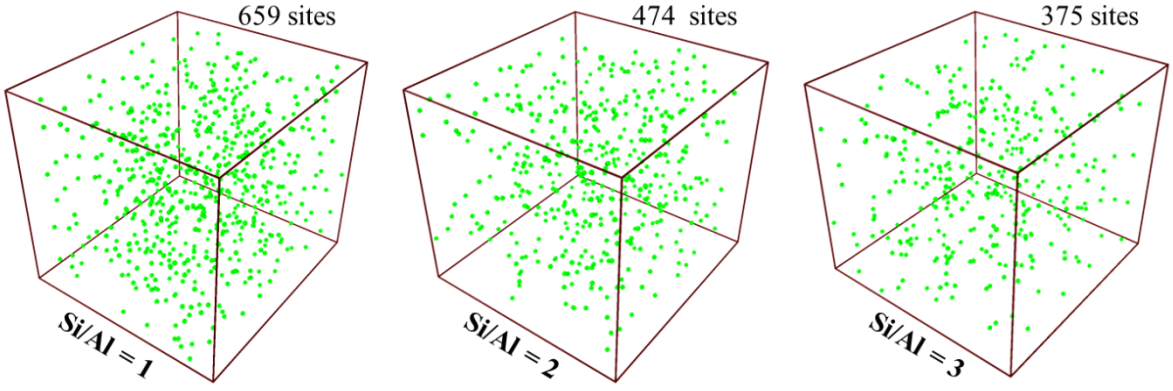

(b) Cross-linking sites in geopolymer matrices

Fig. 5 (a) Snapshots of the cross-linked alumisilicates in geopolymer (Si/Al = 2) model and its internal cross-

linking between oligomers. The green balls represent the cross-linking sites (bridging oxygen atoms) between oligomers; (b) snapshots of the cross-linking sites in geopolymer due to the polymerization of oligomers in geopolymer with Si/Al ratios of 1, 2 and 3. The number of the cross-linking sites is 659, 474 and 375 respectively.

Next, the interfacial atomic structures of geopolymer-aggregate composites are characterized. Fig. 6(a) presents a density field of one composite model with the Si/Al ratio of 3 for geopolymer. It can clearly be seen that there is a low density region at the middle of the composite, which can be defined as an atomic-level "interfacial transition zone (ITZ)". Please note that the other ITZ at the boundary is not labeled where it is also an interface between geopolymer and silica aggregate as periodic boundary conditions are used in this study. The ITZ formation is attributed to the concentration of –OH groups from both geopolymer and silica aggregate, as Fig. 3(c) and 4(a) prove that H-bonding is the major interfacial bonding form. Interfacial H-bonding can generate a region with a density approaching the density of water (1 g/cm^3), which is an H-bonding system. Previously, the atomic-level ITZ with a low density was observed at the interfaces of various campsites, such as cement-polymer composites [80], SiO_2-epoxy composites [81], and hydroxyl functionalized graphene-geopolymer composites [62], which agrees with the present findings. To further characterize the ITZ features of these composites and the effect of the Si/Al ratios of geopolymer, the atomic density profile of the three composite models is plotted in Fig. 6(b) as a function of the distance along the y-direction. The ITZ density of the composites is 1.67 g/cm^3, 1.40 g/cm^3 and 1.29 g/cm^3 respectively, suggesting that the Si/Al ratio plays an important role in the ITZ density. The decrease of ITZ density results from less Na and Al atoms concentrating on the surface of the silica aggregate when the Si/Al ratio increases, as proved in Fig. 4(a). The ITZ widths for the three composites are 3.8 Å, 4.0 Å and 4.0 Å, which shows a very limited increase (~ 5%) with increasing the Si/Al ratio. This indicates that the ITZ width is mainly dependent on the interfacial H-bonding while the concentration change of Na and Al atoms on the surface of silica aggregate has a limited effect with increasing the Si/Al ratio. In conclusion, there is an ITZ between the geopolymer and the silica aggregate and its density is highly correlated with

the Si/Al ratio of geopolymer. However, the ITZ width is not greatly affected such a ratio.

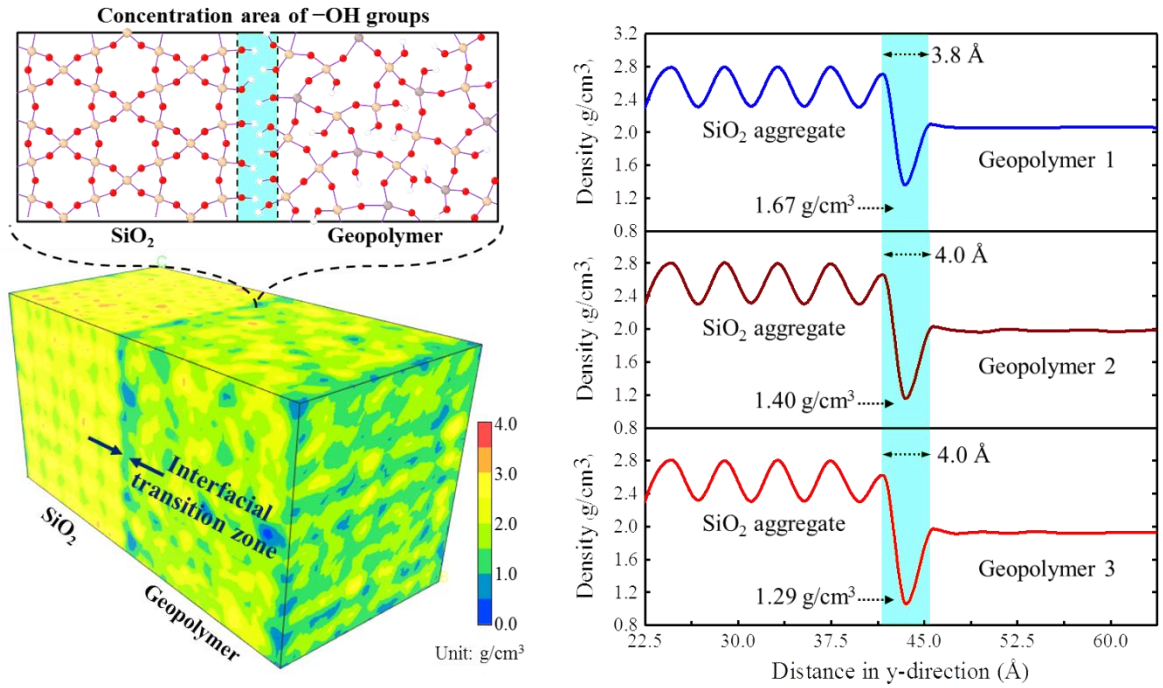

Fig. 6 (a) Density field of a geopolymer-aggregate composite model (Si/Al = 3 for geopolymer) and a schematic view of the concentration of –OH groups at the interface based on the results from Fig. 4. Please note that the interfacial transition zone (ITZ) in the middle is labeled while the other one at the boundary is not labeled; (b) atomic density profiles of the three composites as a function of the distance along y distance with the Si/Al ratios of 1 (geopolymer 1), 2 (geopolymer 2) and 3 (geopolymer 3).

3.2 Diffusion behavior

The diffusion behavior in geopolymer binder, is related to a series of material characteristics, such as ion exchange ability [21], immobilization/leaching of alkali ions [35, 56], self-healing process [46], and creep behaviors [82]. To assess the diffusion behavior of different components (aluminosilicates, Na^+ ions and water molecules) in geopolymer, the geopolymer matrices in the composites are first divided equally into 6 parts, as shown in Fig. 7(a). In view of the symmetry of the composite models due to periodic boundary conditions, these parts can be classified into three regions. Then, the mean squared displacement (MSD), defined as an ensemble average of the deviation of the atom positions with respect to their

reference positions over time, of aluminosilicates, Na^+ ions and water molecules in these regions is calculated as a function of time by the following equation [32],

$$MSD(t) = \langle |\boldsymbol{r}(t) - \boldsymbol{r_0}|^2 \rangle = \frac{1}{N}\sum_{i=1}^{N} |\boldsymbol{r}_i(t) - \boldsymbol{r}_i(0)|^2 \quad (2)$$

where N is the number of atoms to be averaged; vector $\boldsymbol{r}_i(0)$ is the reference position of the i-th atom; and vector $\boldsymbol{r}_i(t)$ is the position of the i-th atom at time t. The MSD of aluminosilicates in geopolymer is represented by the MSD of Si and Al atoms [36, 83]. Based on the MSD calculation, the self-diffusion coefficients of different components in geopolymer are further computed by the following equation [32],

$$D = \frac{1}{6}\lim_{t\to\infty}\frac{MSD(t)}{t} \approx \frac{1}{6}\frac{MSD(t_1) - MSD(t_0)}{t_1 - t_0} \quad (3)$$

where t_1 and t_0 represent the final and initial computing time, respectively.

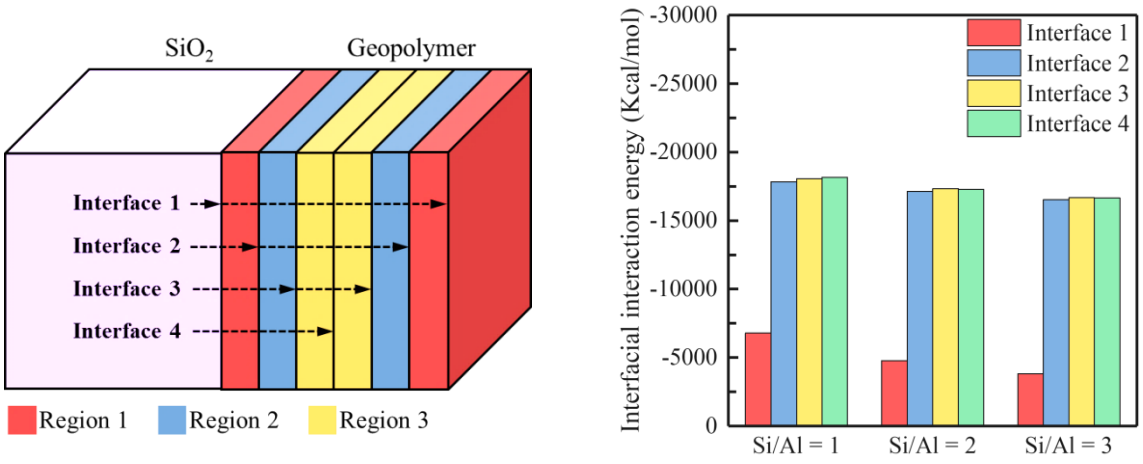

(a) (b)

Fig. 7 (a) Definition of three different regions and four interfaces of geopolymer (Interface 1 is between geopolymer and silica aggregate, and Interface 2, 3 4 are in the geopolymer matrices); (b) interfacial interaction between two adjacent regions.

Fig. 8 summarizes all the MSD curves of aluminosilicates, Na^+ ions and water molecules in different regions of three geopolymer matrices over a time scale of 500 ps. At the very

beginning (< 1 ps, the ballistic motion stage), there is a fast jump from 0 to a certain value for all MSD curves attributed to the inertia of atoms [36], since when MSD values increase slowly with time (the diffusion stage) [35]. All MSD curves suggest that all components, including aluminosilicates, Na^+ ions and water molecules, travel at different rates in different regions of geopolymer matrices, following an order of Region 1 > Region 2 > Region 3. It states that the existence of an interface between geopolymer and silica aggregate can lead to a heterogeneous diffusion characteristic in geopolymer matrices. It is also noted that different components in geopolymer matrices exhibit different diffusion rates, following an order of aluminosilicates < Na^+ ions < water molecules, regardless of Si/Al ratios. It originates from different chemical confinement on these components, because Si and Al atoms in the aluminosilicates of geopolymer are locally covalently bonded with their adjacent atoms (Covalent-bond confinement), and Na^+ ions interact with their adjacent atoms by ionic bonds (Ionic-bond confinement), while water molecules are weakly bonded with other atoms by H-bonds (H-bond confinement) [36]. Additionally, it can be observed that the slope of nearly all the MSD curves decreases slightly with time, which results from the inherent confinement from the solid gel [35].

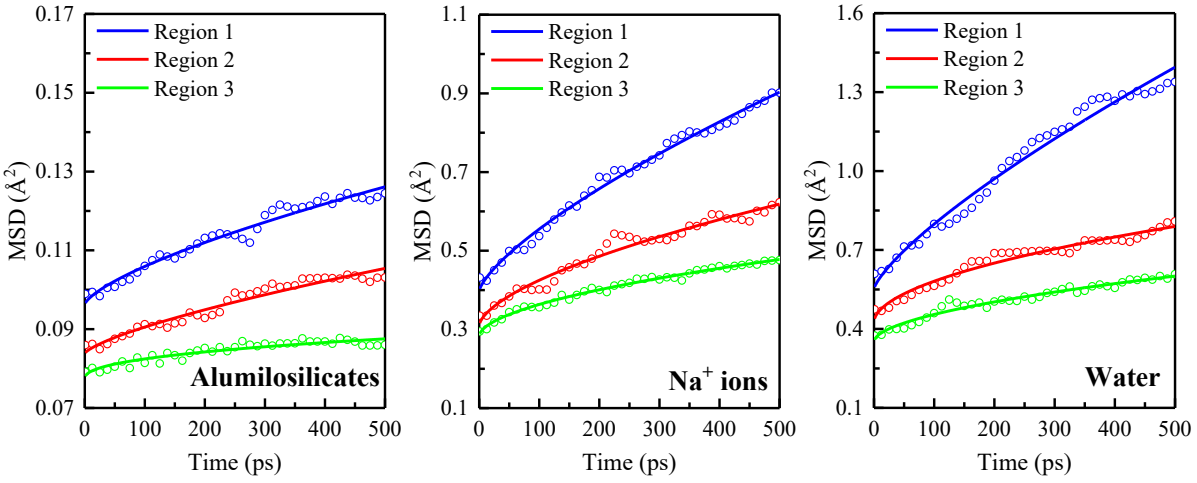

(a) Geopolymer (Si/Al = 1)

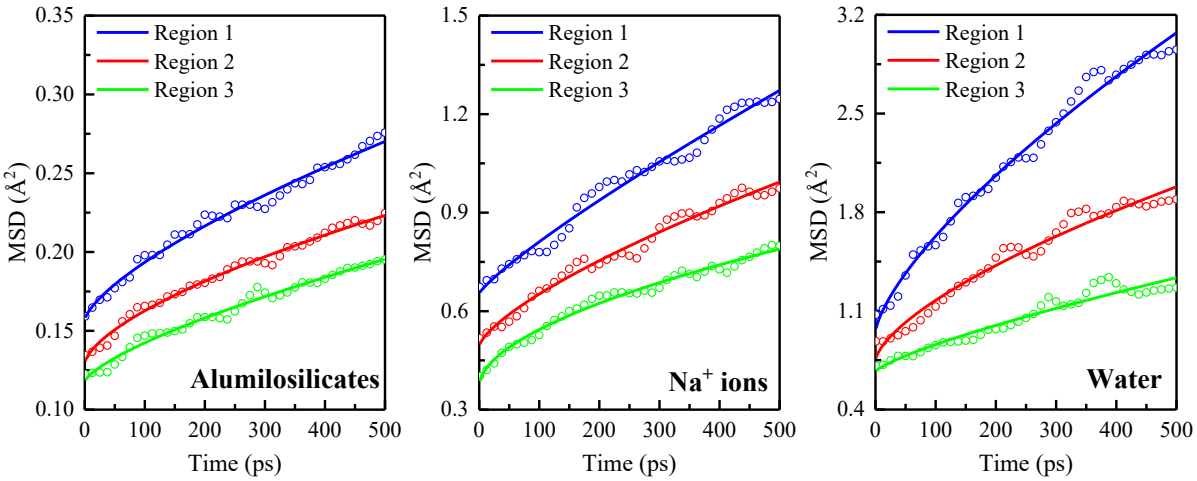

(b) Geopolymer (Si/Al = 2)

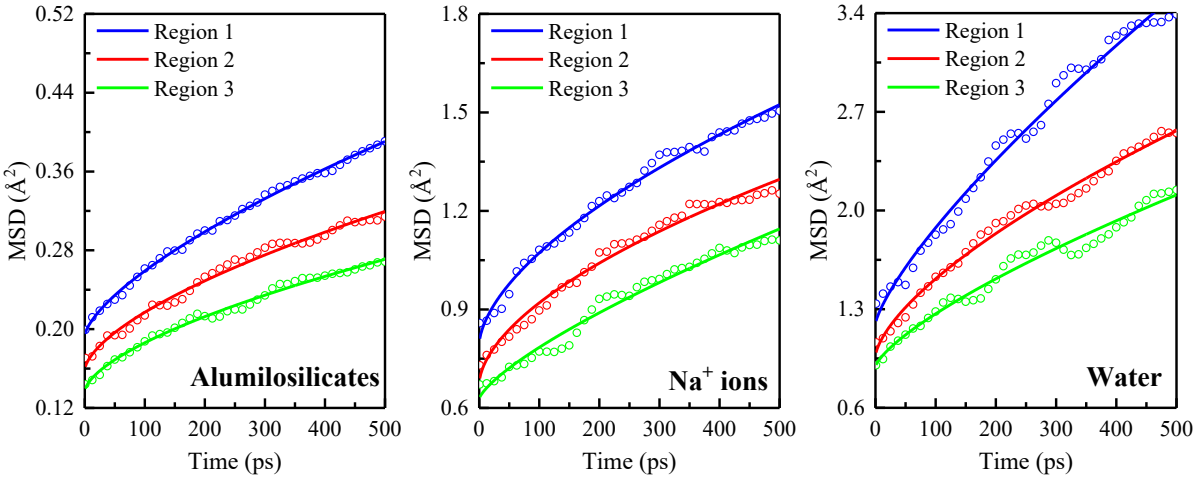

(c) Geopolymer (Si/Al = 3)

Fig. 8 The MSD curves of aluminosilicates, Na^+ ions and water molecules in different regions of geopolymers for three different composites: (a) geopolymer with Si/Al = 1; (b) geopolymer with Si/Al = 2; (c) geopolymer with Si/Al = 3. To show the overall trend of MSD curves with increase of the simulation time, the linear logarithmic transform function ($y = a + bx^c$) was used to fit all curves. Please note that the MSD values at t = 0 should be 0 and there is a marked rise from 0 to a certain value within a short period (< 1 ps, the ballistic motion stage), since when MSD values increase slowly with time (the diffusion stage). Please note we used different y-axis ranges in these figures.

Fig. 9 summarizes all the self-diffusion coefficients of aluminosilicates, Na^+ ions and water molecules in different regions of geopolymer matrices. It is clearly evident that the self-diffusion coefficients of all components are highly affected with the Si/Al ratio of geopolymer

matrices. For example, the increase in Si/Al ratio from 1 to 3 leads to 8.0 times (from 0.08 × 10^{-12} to 0.64 × 10^{-12} m^2/s), 1.4 times (from 1.56 × 10^{-12} to 2.16 × 10^{-12} m^2/s) and 2.8 times (from 2.43 × 10^{-12} to 6.85 × 10^{-12} m^2/s) of increase of the self-diffusion coefficients of aluminosilicates, Na^+ ions and water molecules in Region 1, respectively. Overall, the self-diffusion coefficients of all components in Region 1 obviously exhibit much higher values compared to those in Region 2 and 3, indicating that the diffusion of the components in geopolymer is affected more by the interface between geopolymer and silica aggregate when they are closer to this interface.

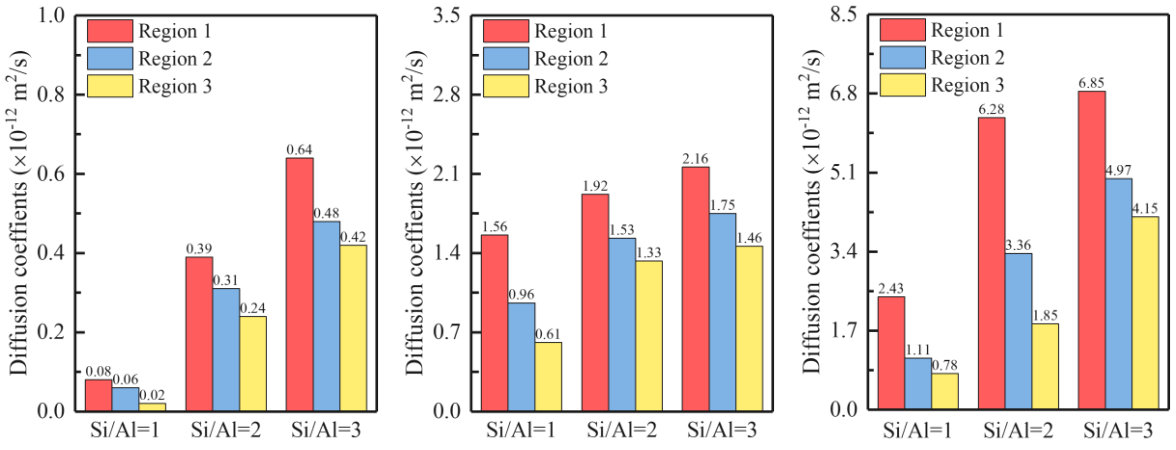

(a) Aluminosilicates (b) Na^+ ions (c) Water

Fig. 9 Summary of the diffusion coefficients of (a) aluminosilicates, (b) Na^+ ions and (c) water in different regions of geopolymers with Si/Al ratios of 1, 2 and 3 for three different composites. Please note we used different y-axis ranges in these figures.

To explain the heterogeneous diffusion characteristics in the geopolymer matrices of the composites and the effect of Si/Al ratio, the interfacial interaction energy between geopolymer and aggregate (Interface 1) and the internal interaction of geopolymer (Interface 2, 3 and 4) are calculated by the following equation to reveal the confinement in different locations of the composites,

$$E_{Interface} = E_{Composite} - E_{Left} - E_{Right} \quad (4)$$

where $E_{composite}$ is the total potential energy of a composite system, E_{left} is the potential energy of the left region of the interface and E_{Right} is the potential energy of the right region

of the interface. The lower interfacial energy corresponds to the stronger interfacial interaction and thus the stronger confinement. The results are recorded in Fig. 7(b). It is obvious that the interfacial interaction energy at Interface 1 is much higher than those at Interface 2, 3 and 4 for all three composites, while there is no notable difference among the interfacial interaction energy at Interfaces 2, 3 and 4. This states that the confinement at the interface (Interface 1) between geopolymer and aggregate is much weaker than the internal confinement within geopolymer while the internal confinement within geopolymer keeps invariant in different locations (Interfaces 2, 3 and 4). Therefore, it can be concluded that the weak interfacial interaction between geopolymer and aggregate is the cause of the heterogeneous diffusion characteristics in the geopolymer matrices of the composites. Additionally, Fig. 7(b) shows that the interfacial interaction energy increases from -6787 Kcal/mol to -3827 Kcal/mol with the Si/Al ratio ranging from 1 to 3, indicating the interfacial interaction is weakened by increasing the Si/Al ratio, in line with the results that less Al-O-Si and Na-O bonds are formed at the interface (Fig. 4). That is to say, the interfacial confinement between geopolymer and aggregate becomes wreaker in case of higher Si/Al ratios, which can be one reason why all components in geopolymer diffuse in a faster rate at higher Si/Al ratios. Another reason is that the increase of Si/Al ratio can decrease the cross-linking degree in geopolymer (Fig. 5), which leads to the weakened confinement between atoms within geopolymer according to the rigid theory and thus promotes the diffusion rate [36, 81, 84, 85].

In conclusion, geopolymer exhibits a heterogeneous diffusion characteristic as its components diffuse at a faster rate at a distance closer to the interface between geopolymer and silica aggregate, resulting from the weak interfacial interaction compared with its internal interaction. The diffusion rate of different components in geopolymer follows an order of aluminosilicates < Na^+ ions < water molecules. Furthermore, the higher Si/Al ratio can cause a faster diffusion of all components in geopolymer, originating from the weakened interfacial interaction and decreased cross-linking degree in geopolymer.

3.3 Mechanical/fracture properties

The interfacial mechanical properties between geopolymer and aggregate are one of the

most noteworthy features that play a decisive role in the material performance of geopolymer concrete [5, 29]. Therefore, a series of tension tests on geopolymer-aggregate composites with a defect at the interface is carried out to investigate the interfacial strength and fracture process. The tensile stress (P_y) is calculated using the following equation during the tensile process [35],

$$P_y = \frac{\sum_k^N m_k v_{k_y} v_{k_y}}{V} + \frac{\sum_k^{N'} r_{k_y} f_{k_y}}{V} \quad (5)$$

where N is the number of atoms in the simulation box; N' denotes the number of atoms in the simulation box and periodic image atoms outside the central box; v_{k_y}, r_{k_y} and f_{k_y} denote the component in the y-direction of the velocity and position of kth atom, and the force exerted on the kth atom; m_k is the mass of the kth atom; and V is the volume of the simulation box.

Fig. 10 (a) exhibits the stress-strain curves of the three geopolymer-aggregate composites. The tensile strength (the peak stress) of the three composites is 4.3 GPa, 1.3 GPa and 0.9 GPa with Si/Al ratio of 1, 2 and 3, respectively. The Young's modulus, determined by calculating the initial slope ratios of the stress-strain curves with the strain ranging from 0.0% to 2.0% [71], is 49.2 GPa, 31.9 GPa and 28.2 GPa for the three composites, respectively. The results indicate that the interfacial strength is weakened by increasing Si/Al ratios. To assess the variation of the interfacial interaction between geopolymer and aggregate during the tensile test, the interfacial interaction energy is calculated based on Eq. (4) and the results are presented in Fig. 10 (b). The initial interfacial interaction energy of the three composites is -6190 Kcal/mol, -4502 Kcal/mol and -3103 Kcal/mol, because of the less Al-O-Si covalent bond and Na-O ionic bonds formed at the interface when the Si/Al ratio increases, as stated previously. That is why a lower Si/Al ratio is more beneficial for the interfacial strength. Similarly, it is widely reported that the interfacial covalent bonding can promote the interfacial stress transfer and thus the interfacial bond strength [36, 62, 81, 86, 87], which is in line with the present study because the concentration of Al-O-Si bonds at the interface is decreased by increasing Si/Al ratios. However, the strongest interface between geopolymer (Si/Al = 1) and aggregate involves the

fastest loss of the interfacial interaction during the tensile process with a maximum loss of ~ 61% at strain = 16%, while the interfacial interaction energy of the composites with the Si/Al ratios of 2 and 3 increases slowly during the tensile process with a maximum loss of ~ 18% at strain = 10% and ~ 33% at strain = 13%, respectively. In addition, there is a recovery stage of the interfacial interaction for all three composites during the tensile process, as revealed from Fig. 10(b). The results indicate that the variation of the interfacial interaction during the tensile process undergoes two stages: the loss stage and recovery stage, and the loss of the interfacial interaction for the three composites follows an order of Si/Al = 1 > Si/Al = 3 > Si/Al = 2.

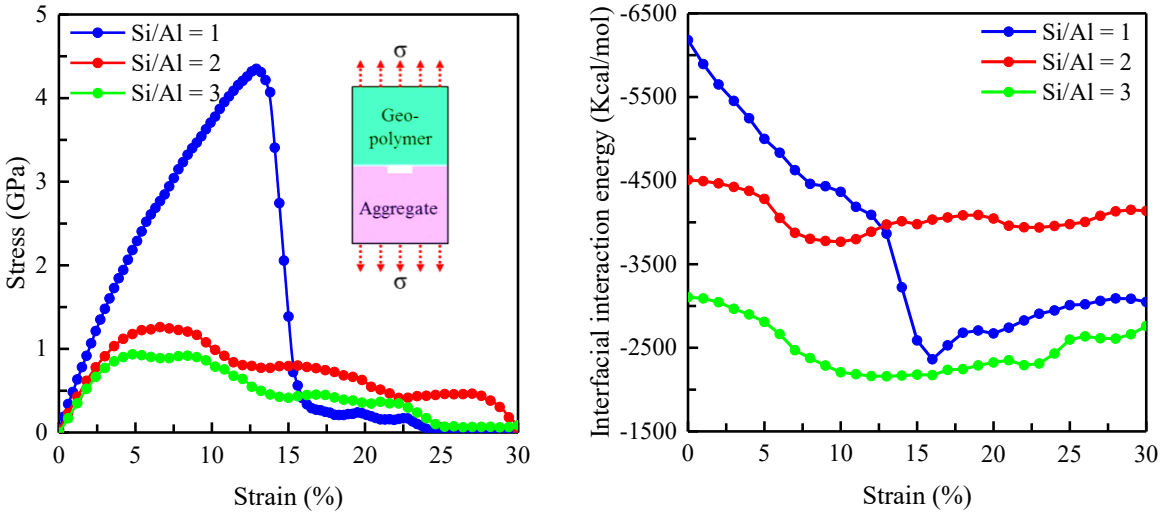

Fig. 10 (a) Tensile stress-strain curves for the geopolymer-aggregate composites with various Si/Al ratios for geopolymer during the tensile process along y direction; (b) the variations of the interfacial interaction energy for the geopolymer-aggregate composites during the tensile process along y direction.

To figure out the interfacial fracture process of geopolymer-aggregate composites, the interfacial chemical bonds, including Al-O-Si, Na-O, and H-bonds, are recorded for the three composites with various Si/Al ratios during the tensile process, as presented in Fig. 11. For the interfacial Al-O-Si bonds, there are 64% and 20% bond breakage for the composites with Si/Al ratios of 1 and 2 during the tensile process, while there is no bond breakage for the composite with the Si/Al ratio of 3, indicating that the interfacial Al-O-Si bonds are more likely to be

broken at lower Si/Al ratios. In addition, no recovery of Al-O-Si bonds is found after the bond breakage. For the interfacial Na-O and H-bonds, the bond number decreases with increasing tensile strain at the initial stage. However, a recovery of Na-O and H-bonds is observed at the interface for all composites at the later stages. Therefore, it can be concluded that the loss stage of the interfacial interaction (Fig. 10 b) originates from the breakage of Al-O-Si, Na-O, and H-bonds at the interface, while the recovery stage is attributed to the recovery of Na-O and H-bonds at the interface. The composite (Si/Al = 1) involves the maximum loss of the interfacial interaction compared with the other two composites due to the fastest breakage of interfacial bonds, while the composite (Si/Al = 2) has the minimum loss of the interfacial interaction because it has the least breakage of Na-O and H-bonds.

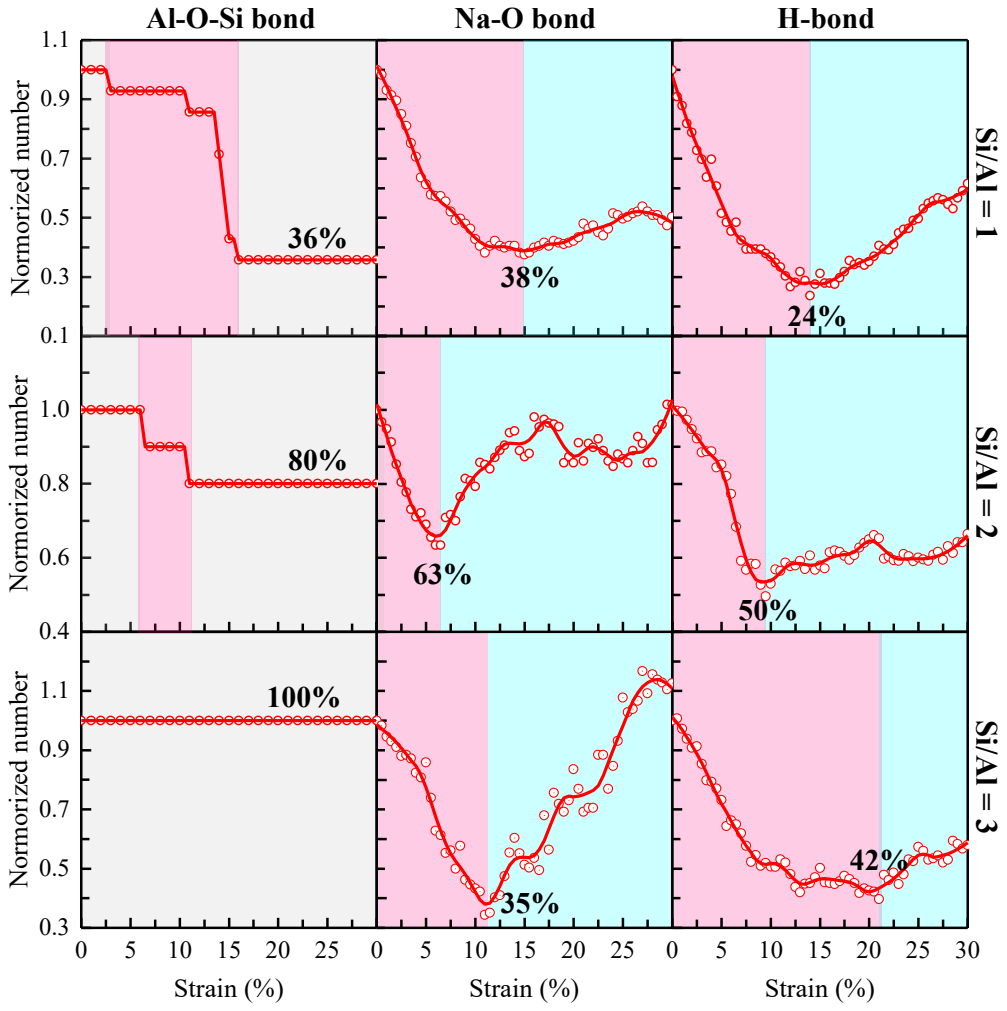

Fig. 11 The record (normalized number) of the interfacial chemical bonds, including Al-O-Si, Na-O, and H-bonds, for the geopolymer-aggregate composites with Si/Al ratios of 1, 2 and 3. The invariable region is

labeled in grey color; the descending region is labeled in pink color; and the ascending region is labeled in blue color.

In order to further understand the fracture process of geopolymer-aggregate composites, Fig. 12 shows a side view of the three composites with various Si/Al ratios for geopolymer under the tensile process. Overall, the fracture process for the three composites undergoes three stages: crack propagation, chain bridging and chain breakage. The main difference is that the formation of the chain bridging and breakage for the composites (Si/Al = 1) is earlier than the other two composites (Si/Al = 2 and 3), in line with the results that the composite (Si/Al = 1) fails first in Fig.10 (a). By comparing Fig. 12 with Fig. 10 (a), it can be found that the chain bridging is the origin of the residual strength of composites. For example, the composite (Si/Al = 1) still has residual strength at strain = 20% (Fig. 10a), by which time the interfacial connection between geopolymer and aggregate is a chain bridging (Fig. 12a). However, at some times the composites fully lose the strength even though the chain bridging is not broken. For example, the composites (Si/Al = 2 and 3) fully lose the strength at strain = 30% and 25% respectively (Fig. 10a), by which time the chain bridging between geopolymer and aggregate still exists (Fig. 12b and c). According to Fig. 11 and 12, it can be found that the fracture process involves the bond breakage at the interface and in geopolymer matrices. The bond breakage in geopolymer matrices results in a small remnant of geopolymer matrices on the aggregate surface.

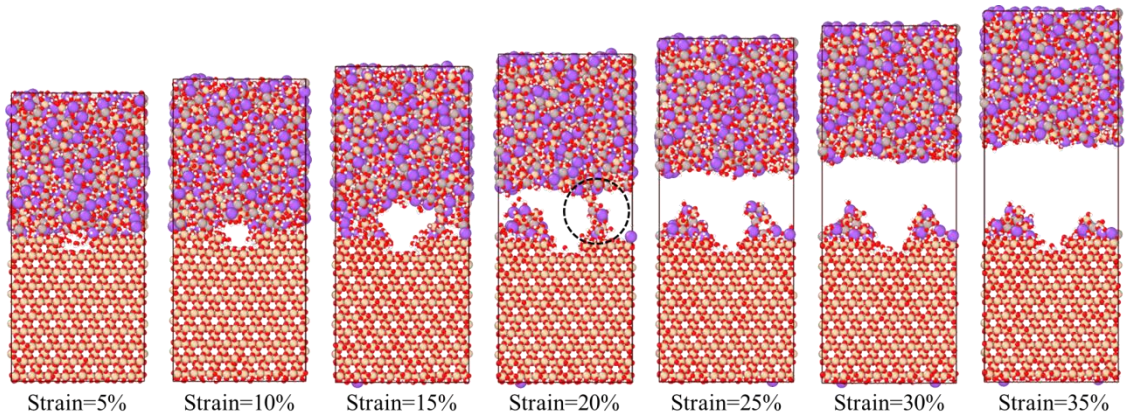

(a) Si/Al ratio = 1

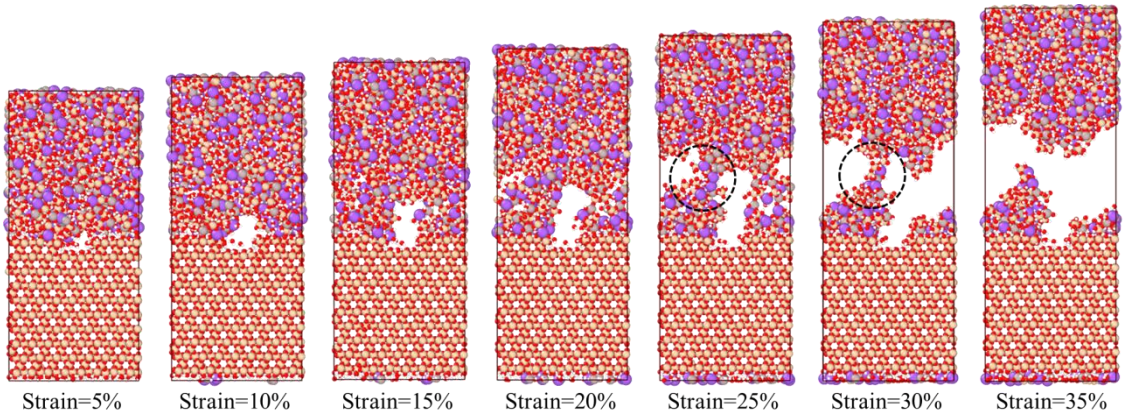

(b) Si/Al ratio = 2

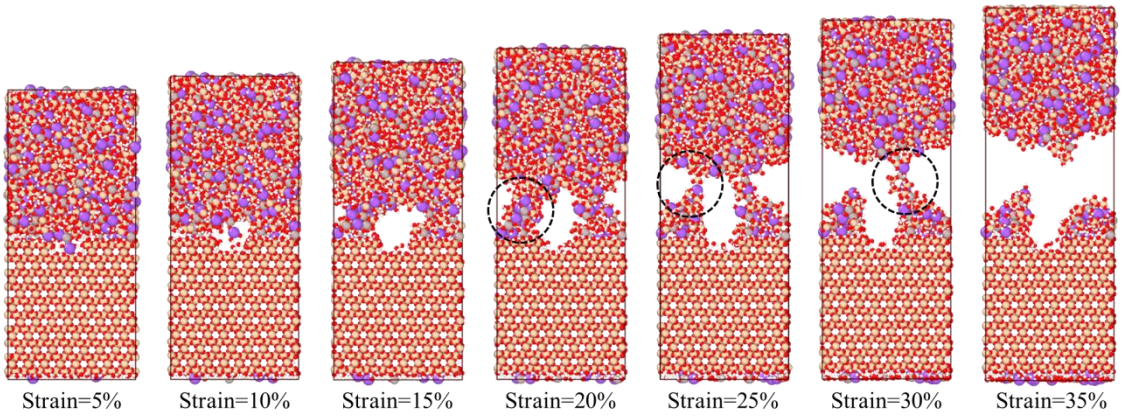

(c) Si/Al ratio = 3

Fig. 12 A side view of the geopolymer-aggregate composites with (a) Si/Al ratio = 1, (b) Si/Al ratio = 2, and (c) Si/Al ratio = 3 during the tensile process. The black circles are used to label the chain bridging between geopolymer and aggregate.

To gain a deep insight into the effect of the chain bridging and breakage on the residual strength of the composites, a series of the local structures of the chains that bridge geopolymer matrices and aggregates are depicted in Fig. 13 at various tensile strains. For the composite (Si/Al = 1), there is an intact aluminosilicate chain that bridges the geopolymer and aggregate at strain = 21.0%, by which time the composite has the residual strength (Fig. 10a). But the aluminosilicate chain is broken and Na^+ ions (sometimes with water molecules) are filled at the breaking point to form a local Na-O ionic bridging (sometimes together with H-bond bridging) at strain = 23.5%, by which time the tensile strength is 0 (Fig. 10a). That is to say, the residual strength of the composite is attributed to the bridging of the aluminosilicate chain while the Na-O ionic bridging (or H-bond bridging) cannot provide the load-bearing ability

517 when the aluminosilicate chain is broken. Finally, the ionic bridging is also broken to form a
518 crack with further increase of the tensile strain. Similarly, the other two composites also
519 undergo two different chain bridging stages: one is the aluminosilicate chain bridging at strain
520 = 27.5% for the composite (Si/Al = 2) and at strain = 23.5% for the composite (Si/Al = 3). At
521 this stage, the composites have the residual strength; and the other is the ionic bridging after
522 the aluminosilicate chains are broken. At this stage, the composites have already lost the
523 strength completely. The results are in line with the fact that Al-O-Si bond strength is much
524 higher than Na-O ionic bond and H-bond strength [88]. It is also another reason why the
525 interfacial strength of the composites is higher at lower Si/Al ratios because geopolymer is
526 more highly cross-linked at lower Si/Al ratios, leading to a stronger geopolymer.

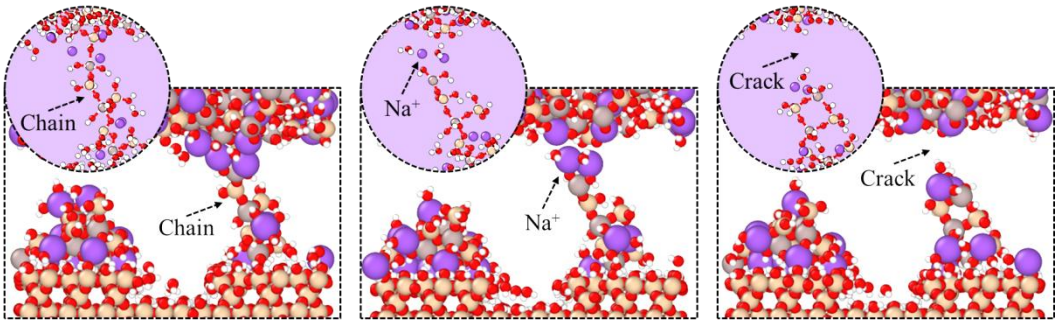

(1) 21.0% strain (2) 23.5% strain (3) 24.0% strain

(a) Si/Al ratio = 1

527

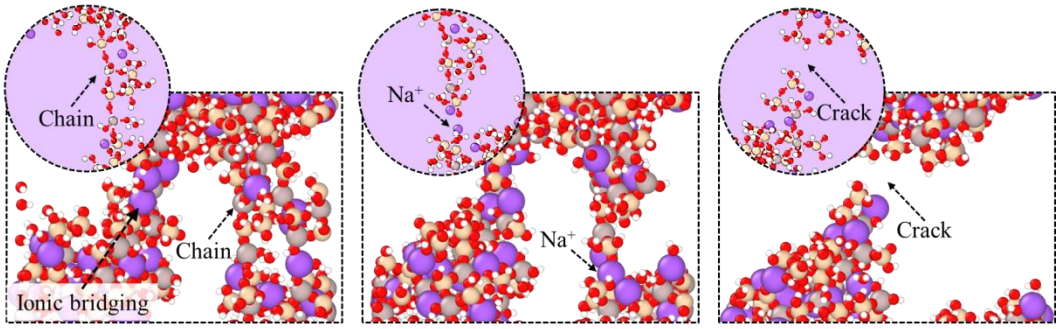

(1) 27.5% strain (2) 29.1% strain (3) 34.8% strain

(b) Si/Al ratio = 2

528

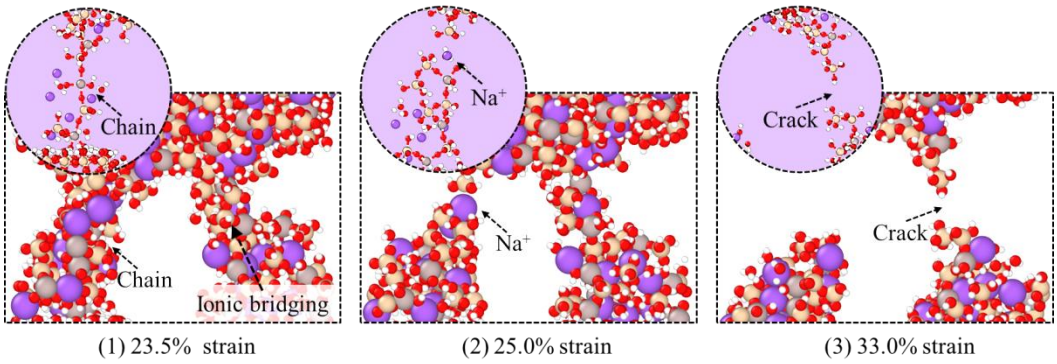

(c) Si/Al ratio = 3

Fig. 13 The local chemical structure of the chains that bridges the geopolymer and aggregate in the composites with (a) Si/Al ratio = 1, (b) Si/Al ratio = 2, and (c) Si/Al ratio = 3 during the tensile process. The images in the circles show again the local structure using the ball-stick models to reveal the chemical bonding of the molecular structure.

In conclusion, lower Si/Al ratios are more beneficial for the interfacial strength of geopolymer-aggregate composites, resulting from more Al-O-Si and Na-O bonds formed at the interface that contribute to the interfacial interaction and a more highly cross-linked aluminosilicate structure. During the tensile process, the variation of the interfacial interaction undergoes two stages: the loss stage formed by the breakage of interfacial bonds, and the recovery stage formed by the recovery of interfacial Na-O and H-bonds. Lower Si/Al ratios can result in faster interfacial Al-O-Si bond breakage. In addition, the fracture process of the composites undergoes three stages: crack propagation, chain bridging and chain breakage. The chain bridging also involves two processes: one is aluminosilicate chain bridging that can contribute to the residual strength of the composites; and the other is Na-O ionic bridging that has no contribution to the strength because ionic bonding is a kind of weak chemical interaction.

4. Conclusions

As a promising sustainable construction material, geopolymer concrete has been poorly understood in terms of the characteristics of geopolymer binder-aggregate interface, especially at the molecular level. In this study, a comprehensive research of atomic-level interfacial properties was carried out, for the first time, using MD simulation with a reactive force field to

550 reveal the chemical events, structure evolution, diffusion behavior and fracture process at the
551 interface between geopolymer (Si/Al = 1, 2, and 3) and SiO_2 aggregate. Some conclusions can
552 be drawn from this study as follows:

553 (1) Chemically, various forms of interfacial bonding are characterized between
554 geopolymer and aggregate, including two types of Al-O-Si bonding formed by the
555 condensation reaction, Na-O ionic bonding and H-bonding. The increase in Si/Al ratio results
556 in lower interfacial Al-O-Si and Na-O bond concentrations, but has a negligible effect on the
557 interfacial H-bond concentration.

558 (2) Structurally, an atomic-level ITZ (low density region) is identified at the interface
559 between geopolymer and aggregate, attributed to the concentration of –OH groups from both
560 SiO_2 aggregate and geopolymer. The ITZ density can be decreased by increasing the Si/Al ratio
561 as less Na and Al atoms concentrate on the surface of the aggregate, but the ITZ width is not
562 greatly affected by the Si/Al ratio, as it is mainly dependent on the interfacial H-bonding.

563 (3) A heterogeneous diffusion characteristic occurs in geopolymer, due to the weak
564 interfacial interaction compared with the internal interaction within geopolymer. The diffusion
565 rate of different components in geopolymer follows an order of aluminosilicates < Na^+ ions <
566 water. The increasing Si/Al ratio can cause a faster diffusion of all components, originating
567 from the weakened interfacial interaction and decreased cross-linking degree of geopolymer.

568 (4) Mechanically, lower Si/Al ratios are more beneficial for the interfacial strength due to
569 the stronger interfacial interaction and more highly cross-linked structure, but result in a faster
570 Al-O-Si bond breakage at the interface. During the tensile process, the variation of the
571 interfacial interaction undergoes two stages: the loss stage due to the breakage of interfacial
572 Al-O-Si, Na-O and H-bonds, and the recovery stage due to the reformation of Na-O and H-
573 bonds.

574 (5) Overall, the fracture process of the geopolymer-aggregate composites undergoes three
575 stages: crack propagation, chain bridging and chain breakage. The chain bridging also involves
576 two processes: one is aluminosilicate chain bridging that can contribute to the residual strength
577 of the composites; and the other is Na-O ionic bridging that cannot contribute to the strength.

Declaration of competing interest

The authors declare that they have no known competing financial interests or personal relationships that could have appeared to influence the work reported in this paper.

Acknowledgments

The authors acknowledge the financial support received from the Hong Kong RGC General Research Fund (Project code: 15223120), the National Natural Science Foundation of China (NSFC) Key Project (Project Code: 51638008), the NSFC/RGC Joint Research Scheme (Project code: N_PolyU542/20), and Innovation Technology Fund (Project code: ITF/077/18FX).

References

[1] R. Hay, K. Celik, Hydration, carbonation, strength development and corrosion resistance of reactive MgO cement-based composites, Cement and Concrete Research 128 (2020) 105941.

[2] A. Attanasio, L. Pascali, V. Tarantino, W. Arena, A. Largo, Alkali-activated mortars for sustainable building solutions: Effect of binder composition on technical performance, Environments 5(3) (2018) 35.

[3] J. Li, W. Zhang, K. Xu, P.J. Monteiro, Fibrillar calcium silicate hydrate seeds from hydrated tricalcium silicate lower cement demand, Cement and Concrete Research 137 (2020) 106195.

[4] I. Ismail, S.A. Bernal, J.L. Provis, R. San Nicolas, S. Hamdan, J.S. van Deventer, Modification of phase evolution in alkali-activated blast furnace slag by the incorporation of fly ash, Cement and Concrete Composites 45 (2014) 125-135.

[5] Z. Luo, W. Li, Y. Gan, K. Mendu, S.P. Shah, Applying grid nanoindentation and maximum likelihood estimation for NASH gel in geopolymer paste: Investigation and discussion, Cement and Concrete Research 135 (2020) 106112.

[6] P. Blanc, A. Lach, A. Lassin, M. Falah, R. Obenaus-Emler, S. Guignot, Modeling hydration of mine tailings: Production of hydraulic binders from alkali-activated materials, Cement and Concrete Research 137 (2020) 106216.

[7] S.A. Bernal, J.L. Provis, R.M. De Gutiérrez, J.S. van Deventer, Accelerated carbonation testing of alkali-activated slag/metakaolin blended concretes: effect of exposure conditions, Materials and Structures 48(3) (2015) 653-669.

[8] O.A. Abdulkareem, M. Ramli, J.C. Matthews, Production of geopolymer mortar system containing high calcium biomass wood ash as a partial substitution to fly ash: An early age evaluation, Composites Part B: Engineering 174 (2019) 106941.

[9] T.M. Pham, Enhanced properties of high-silica rice husk ash-based geopolymer paste by incorporating basalt

613 fibers, Construction and Building Materials 245 (2020) 118422.
614 [10] S.A. Bernal, E.D. Rodríguez, R.M. de Gutiérrez, J.L. Provis, S. Delvasto, Activation of metakaolin/slag
615 blends using alkaline solutions based on chemically modified silica fume and rice husk ash, Waste and Biomass
616 Valorization 3(1) (2012) 99-108.
617 [11] N. Li, C. Shi, Z. Zhang, H. Wang, Y. Liu, A review on mixture design methods for geopolymer concrete,
618 Composites Part B: Engineering 178 (2019) 107490.
619 [12] F. Pacheco-Torgal, J. Castro-Gomes, S. Jalali, Investigations about the effect of aggregates on strength and
620 microstructure of geopolymeric mine waste mud binders, Cement and Concrete Research 37(6) (2007) 933-941.
621 [13] Y.-S. Wang, Y. Alrefaei, J.-G. Dai, Silico-aluminophosphate and alkali-aluminosilicate geopolymers: A
622 comparative review, Frontiers in Materials 6 (2019) 106.
623 [14] F. Puertas, M. Palacios, H. Manzano, J. Dolado, A. Rico, J. Rodríguez, A model for the CASH gel formed in
624 alkali-activated slag cements, Journal of the European Ceramic Society 31(12) (2011) 2043-2056.
625 [15] J.L. Provis, A. Palomo, C. Shi, Advances in understanding alkali-activated materials, Cement and Concrete
626 Research 78 (2015) 110-125.
627 [16] M. Komljenović, G. Tanasijević, N. Džunuzović, J. Provis, Immobilization of cesium with alkali-activated
628 blast furnace slag, Journal of hazardous materials 388 (2020) 121765.
629 [17] S.A. Kearney, B. McLuckie, K. Webb, R. Orr, I.A. Vatter, C.L. Corkhill, M. Hayes, M.J. Angus, J.L. Provis,
630 Effects of plutonium dioxide encapsulation on the physico-chemical development of Portland cement blended
631 grouts, Journal of Nuclear Materials 530 (2020) 151960.
632 [18] M. Lahoti, K.H. Tan, E.-H. Yang, A critical review of geopolymer properties for structural fire-resistance
633 applications, Construction and Building Materials 221 (2019) 514-526.
634 [19] P.K. Sarker, R. Haque, K.V. Ramgolam, Fracture behaviour of heat cured fly ash based geopolymer concrete,
635 Materials & Design 44 (2013) 580-586.
636 [20] H. Peng, C. Cui, C. Cai, Y. Liu, Z. Liu, Microstructure and microhardness property of the interface between
637 a metakaolin/GGBFS-based geopolymer paste and granite aggregate, Construction and Building Materials 221
638 (2019) 263-273.
639 [21] M. Khan, A. Castel, A. Akbarnezhad, S.J. Foster, M. Smith, Utilisation of steel furnace slag coarse aggregate
640 in a low calcium fly ash geopolymer concrete, Cement and Concrete Research 89 (2016) 220-229.
641 [22] S. Demie, M.F. Nuruddin, N. Shafiq, Effects of micro-structure characteristics of interfacial transition zone
642 on the compressive strength of self-compacting geopolymer concrete, Construction and Building Materials 41
643 (2013) 91-98.
644 [23] R. Embong, A. Kusbiantoro, N. Shafiq, M.F. Nuruddin, Strength and microstructural properties of fly ash
645 based geopolymer concrete containing high-calcium and water-absorptive aggregate, Journal of cleaner
646 production 112 (2016) 816-822.
647 [24] W. Lee, J. Van Deventer, The interface between natural siliceous aggregates and geopolymers, Cement and
648 Concrete Research 34(2) (2004) 195-206.
649 [25] Y. Zhang, W. Sun, J. Li, Hydration process of interfacial transition in potassium polysialate (K-PSDS)
650 geopolymer concrete, Magazine of Concrete Research 57(1) (2005) 33-38.
651 [26] V. Sata, A. Wongsa, P. Chindaprasirt, Properties of pervious geopolymer concrete using recycled aggregates,
652 Construction and Building Materials 42 (2013) 33-39.
653 [27] R. Pouhet, M. Cyr, Formulation and performance of flash metakaolin geopolymer concretes, Construction
654 and Building Materials 120 (2016) 150-160.

[28] M. Zhang, N.A. Deskins, G. Zhang, R.T. Cygan, M. Tao, Modeling the polymerization process for geopolymer synthesis through reactive molecular dynamics simulations, The Journal of Physical Chemistry C 122(12) (2018) 6760-6773.
[29] Y.-S. Wang, K.-D. Peng, Y. Alrefaei, J.-G. Dai, The bond between geopolymer repair mortars and OPC concrete substrate: Strength and microscopic interactions, Cement and Concrete Composites 119 (2021) 103991.
[30] L.-Y. Xu, Y. Alrefaei, Y.-S. Wang, J.-G. Dai, Recent advances in molecular dynamics simulation of the NASH geopolymer system: modeling, structural analysis, and dynamics, Construction and Building Materials 276 (2021) 122196.
[31] R.K. Mishra, A.K. Mohamed, D. Geissbühler, H. Manzano, T. Jamil, R. Shahsavari, A.G. Kalinichev, S. Galmarini, L. Tao, H. Heinz, cemff: A force field database for cementitious materials including validations, applications and opportunities, Cement and Concrete Research 102 (2017) 68-89.
[32] E. Duque-Redondo, K. Yamada, H. Manzano, Cs retention and diffusion in CSH at different Ca/Si ratio, Cement and Concrete Research 140 (2021) 106294.
[33] H. Manzano, E. Durgun, I.i. López-Arbeloa, J.C. Grossman, Insight on tricalcium silicate hydration and dissolution mechanism from molecular simulations, ACS applied materials & interfaces 7(27) (2015) 14726-14733.
[34] F. Lolli, H. Manzano, J.L. Provis, M.C. Bignozzi, E. Masoero, Atomistic simulations of geopolymer models: the impact of disorder on structure and mechanics, ACS applied materials & interfaces 10(26) (2018) 22809-22820.
[35] M.F. Kai, L.W. Zhang, K.M. Liew, Atomistic insights into structure evolution and mechanical property of calcium silicate hydrates influenced by nuclear waste caesium, Journal of Hazardous Materials 411 (2021) 125033.
[36] M. Kai, L. Zhang, K. Liew, Carbon nanotube-geopolymer nanocomposites: A molecular dynamics study of the influence of interfacial chemical bonding upon the structural and mechanical properties, Carbon 161 (2020) 772-783.
[37] L. Chu, L. Luo, T. Fwa, Effects of aggregate mineral surface anisotropy on asphalt-aggregate interfacial bonding using molecular dynamics (MD) simulation, Construction and Building Materials 225 (2019) 1-12.
[38] M. Huang, H. Zhang, Y. Gao, L. Wang, Study of diffusion characteristics of asphalt–aggregate interface with molecular dynamics simulation, International Journal of Pavement Engineering (2019) 1-12.
[39] G. Xu, H. Wang, Study of cohesion and adhesion properties of asphalt concrete with molecular dynamics simulation, Computational Materials Science 112 (2016) 161-169.
[40] G. Xu, H. Wang, Molecular dynamics study of oxidative aging effect on asphalt binder properties, Fuel 188 (2017) 1-10.
[41] M. Xu, J. Yi, D. Feng, Y. Huang, D. Wang, Analysis of adhesive characteristics of asphalt based on atomic force microscopy and molecular dynamics simulation, ACS applied materials & interfaces 8(19) (2016) 12393-12403.
[42] H. Wang, E. Lin, G. Xu, Molecular dynamics simulation of asphalt-aggregate interface adhesion strength with moisture effect, International Journal of Pavement Engineering 18(5) (2017) 414-423.
[43] Z. Dong, Z. Liu, P. Wang, X. Gong, Nanostructure characterization of asphalt-aggregate interface through molecular dynamics simulation and atomic force microscopy, Fuel 189 (2017) 155-163.
[44] G. Xu, H. Wang, Molecular dynamics study of interfacial mechanical behavior between asphalt binder and mineral aggregate, Construction and Building Materials 121 (2016) 246-254.
[45] Y. Lu, L. Wang, Nanoscale modelling of mechanical properties of asphalt–aggregate interface under tensile

loading, International Journal of Pavement Engineering 11(5) (2010) 393-401.
[46] H. Yao, Q. Dai, Z. You, Investigation of the asphalt–aggregate interaction using molecular dynamics, Petroleum Science and Technology 35(6) (2017) 586-593.
[47] J. Rimsza, J. Du, Interfacial structure and evolution of the water–silica gel system by reactive force-field-based molecular dynamics simulations, The Journal of Physical Chemistry C 121(21) (2017) 11534-11543.
[48] S. Li, Y. Chen, J. Zhao, C. Wang, N. Wei, Atomic structure causing an obvious difference in thermal conductance at the Pd–H 2 O interface: a molecular dynamics simulation, Nanoscale 12(34) (2020) 17870-17879.
[49] Y. Bai, H. Sui, X. Liu, L. He, X. Li, E. Thormann, Effects of the N, O, and S heteroatoms on the adsorption and desorption of asphaltenes on silica surface: A molecular dynamics simulation, Fuel 240 (2019) 252-261.
[50] M. Ebadi, L.T. Costa, C.M. Araujo, D. Brandell, Modelling the Polymer Electrolyte/Li-Metal Interface by Molecular Dynamics Simulations, Electrochimica Acta 234 (2017) 43-51.
[51] W. Peng, K. Sun, R. Abdullah, M. Zhang, J. Chen, J. Shi, Strengthening mechanisms of graphene coatings on Cu film under nanoindentation: a molecular dynamics simulation, Applied Surface Science 487 (2019) 22-31.
[52] M.M. Koleini, M.F. Mehraban, S. Ayatollahi, Effects of low salinity water on calcite/brine interface: A molecular dynamics simulation study, Colloids and Surfaces A: Physicochemical and Engineering Aspects 537 (2018) 61-68.
[53] W. Sun, H. Wang, Moisture effect on nanostructure and adhesion energy of asphalt on aggregate surface: A molecular dynamics study, Applied Surface Science 510 (2020) 145435.
[54] L. Zhuravlev, The surface chemistry of amorphous silica. Zhuravlev model, Colloids and Surfaces A: Physicochemical and Engineering Aspects 173(1-3) (2000) 1-38.
[55] L. Zhuravlev, Concentration of hydroxyl groups on the surface of amorphous silicas, Langmuir 3(3) (1987) 316-318.
[56] M.R. Sadat, S. Bringuier, A. Asaduzzaman, K. Muralidharan, L. Zhang, A molecular dynamics study of the role of molecular water on the structure and mechanics of amorphous geopolymer binders, The Journal of chemical physics 145(13) (2016) 134706.
[57] S. Nosé, A unified formulation of the constant temperature molecular dynamics methods, The Journal of chemical physics 81(1) (1984) 511-519.
[58] W.G. Hoover, Canonical dynamics: Equilibrium phase-space distributions, Physical review A 31(3) (1985) 1695.
[59] M.R. Sadat, K. Muralidharan, L. Zhang, Reactive molecular dynamics simulation of the mechanical behavior of sodium aluminosilicate geopolymer and calcium silicate hydrate composites, Computational Materials Science 150 (2018) 500-509.
[60] Y. Zhang, J.L. Zhang, J.Y. Jiang, D.S. Hou, J.R. Zhang, The effect of water molecules on the structure, dynamics, and mechanical properties of sodium aluminosilicate hydrate (NASH) gel: A molecular dynamics study, Construction and Building Materials 193 (2018) 491-500.
[61] A.C. Van Duin, S. Dasgupta, F. Lorant, W.A. Goddard, ReaxFF: a reactive force field for hydrocarbons, The Journal of Physical Chemistry A 105(41) (2001) 9396-9409.
[62] L. Zhang, M. Kai, X. Chen, Si-doped graphene in geopolymer: Its interfacial chemical bonding, structure evolution and ultrastrong reinforcing ability, Cement and Concrete Composites 109 (2020) 103522.
[63] K. Chenoweth, A.C. Van Duin, W.A. Goddard, ReaxFF reactive force field for molecular dynamics simulations of hydrocarbon oxidation, The Journal of Physical Chemistry A 112(5) (2008) 1040-1053.
[64] K.L. Joshi, G. Psofogiannakis, A.C. Van Duin, S. Raman, Reactive molecular simulations of protonation of

water clusters and depletion of acidity in H-ZSM-5 zeolite, Physical Chemistry Chemical Physics 16(34) (2014) 18433-18441.
[65] D.-C. Yue, T.-B. Ma, Y.-Z. Hu, J. Yeon, A.C. van Duin, H. Wang, J. Luo, Tribochemistry of phosphoric acid sheared between quartz surfaces: A reactive molecular dynamics study, The Journal of Physical Chemistry C 117(48) (2013) 25604-25614.
[66] D.-C. Yue, T.-B. Ma, Y.-Z. Hu, J. Yeon, A.C. van Duin, H. Wang, J. Luo, Tribochemical mechanism of amorphous silica asperities in aqueous environment: a reactive molecular dynamics study, Langmuir 31(4) (2015) 1429-1436.
[67] G.M. Psofogiannakis, J.F. McCleerey, E. Jaramillo, A.C. Van Duin, ReaxFF reactive molecular dynamics simulation of the hydration of Cu-SSZ-13 zeolite and the formation of Cu dimers, The Journal of Physical Chemistry C 119(12) (2015) 6678-6686.
[68] M.C. Pitman, A.C. Van Duin, Dynamics of confined reactive water in smectite clay–zeolite composites, Journal of the American Chemical Society 134(6) (2012) 3042-3053.
[69] J.L. Suter, L. Kabalan, M. Khader, P.V. Coveney, Ab initio molecular dynamics study of the interlayer and micropore structure of aqueous montmorillonite clays, Geochimica et Cosmochimica Acta 169 (2015) 17-29.
[70] M.A. Qomi, K. Krakowiak, M. Bauchy, K. Stewart, R. Shahsavari, D. Jagannathan, D.B. Brommer, A. Baronnet, M.J. Buehler, S. Yip, Combinatorial molecular optimization of cement hydrates, Nature communications 5 (2014) 4960.
[71] M.F. Kai, L.W. Zhang, K.M. Liew, Graphene and graphene oxide in calcium silicate hydrates: Chemical reactions, mechanical behaviors and interfacial sliding, Carbon 146 (2019) 181-193.
[72] Y. Yu, B. Wang, M. Wang, G. Sant, M. Bauchy, Reactive molecular dynamics simulations of sodium silicate glasses—toward an improved understanding of the structure, International Journal of Applied Glass Science 8(3) (2017) 276-284.
[73] R. Dongol, L. Wang, A. Cormack, S. Sundaram, Molecular dynamics simulation of sodium aluminosilicate glass structures and glass surface-water reactions using the reactive force field (ReaxFF), Applied Surface Science 439 (2018) 1103-1110.
[74] M. Ravi, V.L. Sushkevich, J.A. van Bokhoven, Towards a better understanding of Lewis acidic aluminium in zeolites, Nature Materials 19(10) (2020) 1047-1056.
[75] S. Yong, D. Feng, G. Lukey, J. Van Deventer, Chemical characterisation of the steel–geopolymeric gel interface, Colloids and Surfaces A: Physicochemical and Engineering Aspects 302(1-3) (2007) 411-423.
[76] C. Liu, P. Huang, Role of hydroxy-aluminosilicate ions (proto-imogolite sol) in the formation of humic substances, Organic Geochemistry 33(3) (2002) 295-305.
[77] W.-M. Ji, L.-W. Zhang, K. Liew, Understanding interfacial interaction characteristics of carbon nitride reinforced epoxy composites from atomistic insights, Carbon 171 (2021) 45-54.
[78] J. Li, W. Zhang, K. Garbev, G. Beuchle, P.J. Monteiro, Influences of cross-linking and Al incorporation on the intrinsic mechanical properties of tobermorite, Cement and Concrete Research 136 (2020) 106170.
[79] T. Hanzlíček, I. Perná, K. Uličná, V. Římal, H. Štěpánková, The Evaluation of Clay Suitability for Geopolymer Technology, Minerals 10(10) (2020) 852.
[80] D. Hou, J. Yu, P. Wang, Molecular dynamics modeling of the structure, dynamics, energetics and mechanical properties of cement-polymer nanocomposite, Composites Part B: Engineering 162 (2019) 433-444.
[81] Z.K. Wang, Q. Lv, S.H. Chen, C.L. Li, S.Q. Sun, S.Q. Hu, Effect of interfacial bonding on interphase properties in SiO2/epoxy nanocomposite: a molecular dynamics simulation study, ACS applied materials &

781 interfaces 8(11) (2016) 7499-7508.
782 [82] M.F. Kai, L.W. Zhang, K.M. Liew, New insights into creep characteristics of calcium silicate hydrates at
783 molecular level, Cement and Concrete Research 142 (2021) 106366.
784 [83] D. Hou, Y. Zhang, T. Yang, J. Zhang, H. Pei, J. Zhang, J. Jiang, T. Li, Molecular structure, dynamics, and
785 mechanical behavior of sodium aluminosilicate hydrate (NASH) gel at elevated temperature: a molecular
786 dynamics study, Physical Chemistry Chemical Physics 20(31) (2018) 20695-20711.
787 [84] M. Bauchy, M.J.A. Qomi, C. Bichara, F.-J. Ulm, R.J.-M. Pellenq, Rigidity transition in materials: hardness
788 is driven by weak atomic constraints, Physical review letters 114(12) (2015) 125502.
789 [85] M. Bauchy, M.J. Abdolhosseini Qomi, C. Bichara, F.-J. Ulm, R.J.-M. Pellenq, Nanoscale structure of cement:
790 viewpoint of rigidity theory, The Journal of Physical Chemistry C 118(23) (2014) 12485-12493.
791 [86] J. Lu, M. Luo, B.I. Yakobson, Glass composites reinforced with silicon-doped carbon nanotubes, Carbon 128
792 (2018) 231-236.
793 [87] W. Ji, L. Zhang, Diamond nanothread reinforced polymer composites: ultra-high glass transition temperature
794 and low density, Composites Science and Technology 183 (2019) 107789.
795 [88] G.A. Lyngdoh, S. Nayak, R. Kumar, N. Anoop Krishnan, S. Das, Fracture toughness of sodium
796 aluminosilicate hydrate (NASH) gels: Insights from molecular dynamics simulations, Journal of Applied Physics
797 127(16) (2020) 165107.
798